Materials Today Bio 23 (2023) 100875

Contents lists available at ScienceDirect

Materials Today Bio

journal homepage: www.journals.elsevier.com/materials-today-bio

Natural self-healing injectable hydrogels loaded with exosomes and berberine for infected wound healing

Pu Yang [a], Yikun Ju [a], Xiangjun Liu [a], Zhen Li [a], Hairong Liu [b], Mengni Yang [b], Xin Chen [b], Lanjie Lei [c,**], Bairong Fang [a,*]

[a] Department of Plastic and Aesthetic (Burn) Surgery, The Second Xiangya Hospital, Central South University, Changsha, 410011, Hunan, China
[b] College of Materials Science and Engineering, Hunan University, Changsha, 410082, Hunan, China
[c] Institute of Translational Medicine, Zhejiang Shuren University, Hangzhou, 310015, Zhejiang, China

ARTICLE INFO

Keywords:
Self-healing hydrogels
Natural polysaccharides
Infected wounds
Exosomes
Berberine

ABSTRACT

Complete and rapid healing of infected skin wounds remains a challenge in current clinical treatment. In this study, we prepared a self-healing injectable CK hydrogel by crosslinking two natural polysaccharides, carboxymethyl chitosan and oxidized konjac glucomannan, based on the Schiff base bond. To enhance the biological function of the hydrogel, we multi-functionalized hydrogen by loading it with berberine (BBR) and stem cell-derived exosomes (Exo), forming a composite hydrogel, CK@BBR&Exo, which could be injected directly into the wound through a needle and adhered to the wound. Furthermore, the self-healing properties of CK@BBR&Exo increased its usefulness and service life. Additionally, the drug-loaded CK@BBR&Exo hydrogel was versatile, inhibiting bacterial growth, regulating the inflammatory response, and promoting neovascularization in infected skin wounds, thus achieving the rapid healing of infected skin wounds. These results suggest that the CK@BBR&Exo-injectable self-healing hydrogel is an ideal dressing for treating infected skin wounds.

1. Introduction

The skin is the body's largest organ and the first line of defense against external stimuli [1]. Skin trauma is caused by single or multiple factors, such as external forces, electrical currents, chemical substances, and local blood circulation disorders, resulting in partial loss of skin tissue and destruction of skin integrity [2,3]. Skin wound healing is a relatively complex physiological process that involves three main phases: inflammation, proliferation, and remodeling, where multiple cell types, cytokines, and extracellular matrix act synergistically to achieve complete wound healing [4–6]. During the healing process, inevitable complications, such as bleeding and infection, can significantly delay normal wound healing and endanger the patient's life [7–9]. Currently, gauze dressings combined with antibiotic preparations are primarily used to treat infected skin wounds. However, the low suitability of single-formulation dressings for wounds and resistance caused by antibiotic abuse render the current clinical treatment of infected skin wounds ineffective [10,11]. Hydrogel dressings are a promising strategy for wound treatment. A variety of natural biomaterials can be used to construct hydrogels for tissue repair, such as hyaluronic acid and proteins [12,13]. The excellent adhesion and hydrophilicity of hydrogels enable them to adhere rapidly to wounds, stop bleeding, and provide a moist microenvironment that facilitates wound healing. Furthermore, hydrogels are natural drug delivery systems capable of loading various bioactive drugs for wound repair, thereby accelerating full healing [14–16].

Self-repairing hydrogels are special hydrogels formed by reversible physical and chemical bonding. Besides possessing the basic hydrophilic, adhesive, and drug-carrying properties of traditional hydrogels, they can repair themselves rapidly after hydrogel damage and maintain drug-release properties [17–19]. Self-repairing hydrogels based on natural materials are more bio-destructive than synthetic materials and have biological properties that can effectively promote wound healing [20]. Chitosan, a cationic polysaccharide extracted from marine arthropods, can kill bacteria through its cationic action [21,22]. Furthermore, the amino group carried by chitosan can form a Schiff base bond

* Corresponding author.
** Corresponding author.
E-mail addresses: leilanjie1988@163.com (L. Lei), fbrfbr2004@csu.edu.cn (B. Fang).

https://doi.org/10.1016/j.mtbio.2023.100875
Received 24 August 2023; Received in revised form 7 November 2023; Accepted 17 November 2023
Available online 19 November 2023

with the aldehyde groups of other substances and crosslink to form self-repairing hydrogels [18]. Konjac glucomannan (KGM) is a high-molecular-weight hydrophilic polysaccharide obtained from konjac tubers. It is widely used in food chemistry research because of its good biocompatibility and nutritional value; however, relatively little research has been conducted on its application in wound repair [23]. Wang et al. developed a hydrogel with good tissue adhesion, injectability, self-healing, and antibacterial properties by reacting the amino group of chitosan with the aldehyde group of oxidized KGM (OKGM) and loading Ag nanoparticles. The hydrogel could effectively treat irregular wounds [24]. What's more, as a natural macromolecular polysaccharide, KGM possesses good biocompatibility. Moreover, KGM can form a stable hydrogel by cross-linking with carboxymethyl chitosan (CMCS) at a low concentration. Moreover, the loose porosity of KGM after the formation of hydrogels facilitates the loading of drugs and the attachment of cellular components [25,26].

Berberine (BBR) is an isoquinoline alkaloid extracted from *Berberis*, *Phellodendron*, and Canadian water hyacinth. It has good antibacterial, anti-inflammatory, antioxidant, and other biological properties with no apparent side effects [27–29]. Its excellent broad-spectrum antibacterial action and specific biological functions make it more suitable than single clinical antibiotics for repairing infected skin wounds. Notably, the inflammatory response and difficulty in vascular regeneration due to bacterial activity in skin wounds during infection are the main obstacles in wound healing. Exosomes (Exos) are nanoscale lipid-encapsulated structures, with diameters ranging from 30 to 150 nm, that are widely found in body fluids and are internally encapsulated with proteins, mRNA, and microRNA. Exos can achieve rapid wound healing by regulating trauma inflammatory activity, promoting trauma angiogenesis, and accelerating skin cell proliferation and re-epithelialization [30–32]. Many studies have shown that hydrogel-loaded Exos can be used to repair various tissues [32–34].

In this study, we prepared a self-healing hydrogel (CK) based on CMCS crosslinked with KGM Schiff base bonds. Additionally, we multifunctionalized CK by loading BBR and Exo (CK@BBR&Exo) to promote the healing of infected skin wounds (Fig. 1). Next, we measured the physicochemical, rheological, and self-healing properties of CK@BBR&Exo hydrogels. Additionally, we evaluated the potential of CK@BBR&Exo composite hydrogel in infected skin wounds through several experiments, including *in vitro* antibacterial, angiogenesis, and cell migration assays and a rat-infected wound model.

2. Results and discussion

2.1. Characterization of hydrogels

2.1.1. Fourier transform infrared analysis

CK hydrogels are crosslinked based on the Schiff base reaction; thus,

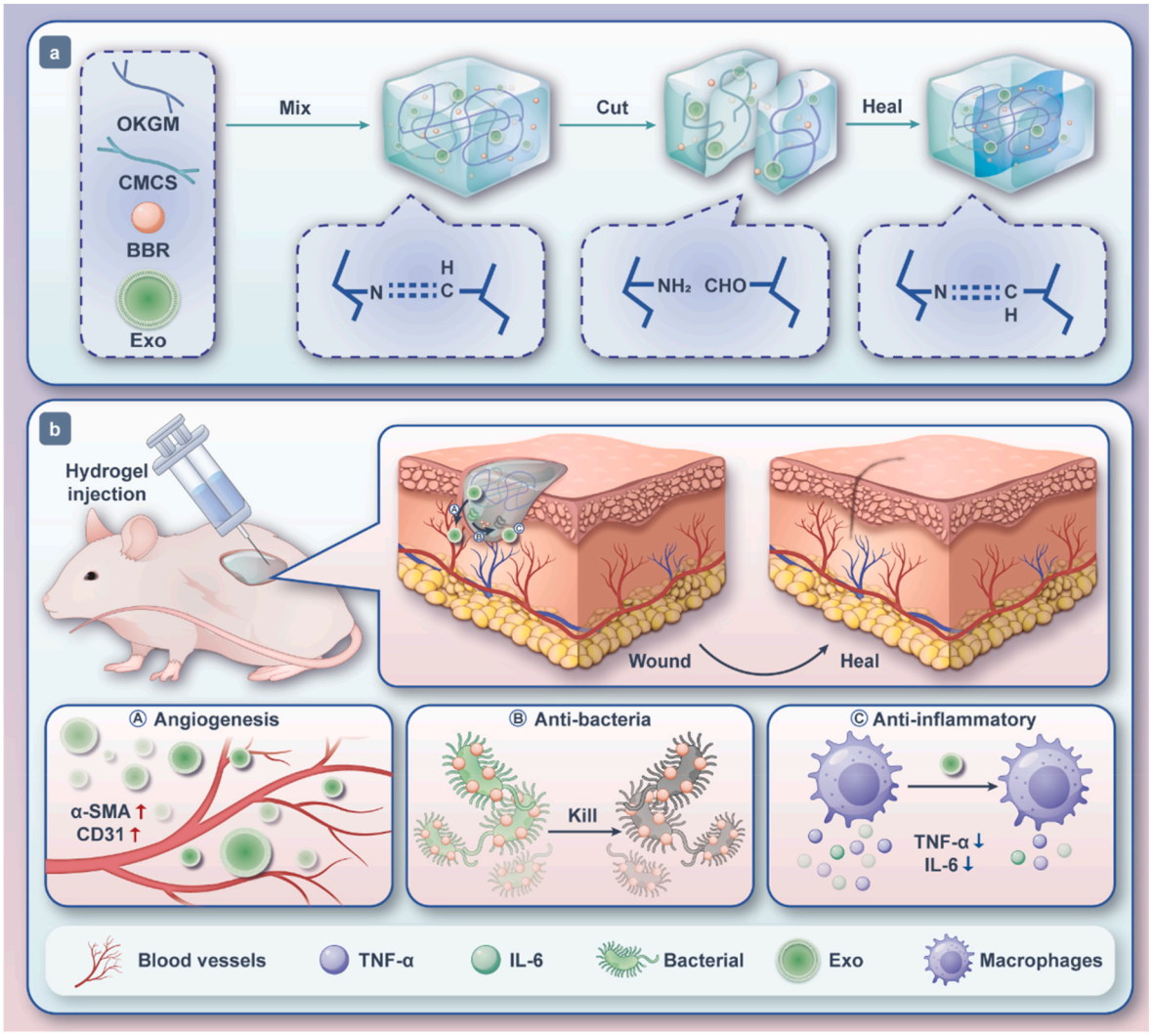

Fig. 1. Schematic illustration of CK@BBR&Exo for infected skin wound repair. (a) Synthesis of CK@BBR&Exo with self-healing properties. (b) Mechanism of action of the injectable hydrogel CK@BBR&Exo.

the oxidation of KGM in them determines the success of the crosslinking. To determine the oxidation of KGM considering the crosslinking of hydrogels, Fourier transform infrared (FTIR) was used to characterize the lyophilized powders of KGM and OKGM (Fig. S1). In the FTIR spectrum of KGM, the peak at 1745 cm^{-1} corresponds to the C–O stretching vibration of the acetyl group. Compared with KGM, the OKGM spectrum showed two considerable absorption peaks at 1730 and 890 cm^{-1}, representing the formation of nascent aldehyde groups, and the successful oxidation of KGM to OKGM, respectively.

2.1.2. Nuclear magnetic resonance analysis

We refer to previous reference for detection methods [35]. We analyzed the characteristic peak spectrum of OKGM using nuclear magnetic resonance (NMR), and the detection results were consistent with previous reference (Fig. S2). The results of this experiment confirmed the important structural formula in the obtained OKGM.

2.1.3. Macro-gel performance of hydrogels

As hydrogels used on traumatic surfaces are directly exposed to external factors, and the slow gelation process can lead to the loss of liquid hydrogel with changes in patient position, hydrogel materials applied to skin trauma should gel rapidly. The OKGM in the hydrogel is a high molecular oxidized polysaccharide that can rapidly form stable Schiff base covalent crosslinks with CMCS at a low concentration. The rapid and stable cross-linking of CK hydrogels facilitates their use in skin wounds. The CK hydrogels could gel spontaneously without intervention at 25 °C (Fig. 2a). The crosslinked hydrogel exhibited macroscopic injectability (Fig. 2b), facilitating its direct application to skin trauma. Furthermore, cut marks were observed on hydrogels cut from different sources when in contact with each other. After 4 h without additional intervention, the two hydrogels adhered together, and no visible cut marks were observed. Pulling two hydrogels of different origins using forceps showed that both were well fused and that the broken ends could withstand external stretching (Fig. 2b).

2.1.4. Morphological characteristics of hydrogels

Hydrogel pore size affects cell proliferation and interaction. The larger the pore size, the more favorable the proliferation and growth of cells. OKGM, as a derivative of a macromolecular natural polysaccharide, crosslinks to form a hydrogel with stable, loose pores. This is equally favorable for its loading for drugs and the attachment of Exos in this study. The external morphology and pore size of the CK hydrogels were directly observed using scanning electron microscopy (Fig. 2c), revealing that the hydrogels were uniformly sized porous frameworks, favorable for the growth and proliferation of skin tissue cells, such as epithelial cells.

2.1.5. Swelling and degradation performance of hydrogels

An ideal hydrogel for trauma applications should have sufficient hydrophilic and swelling properties to adequately fill trauma defects,

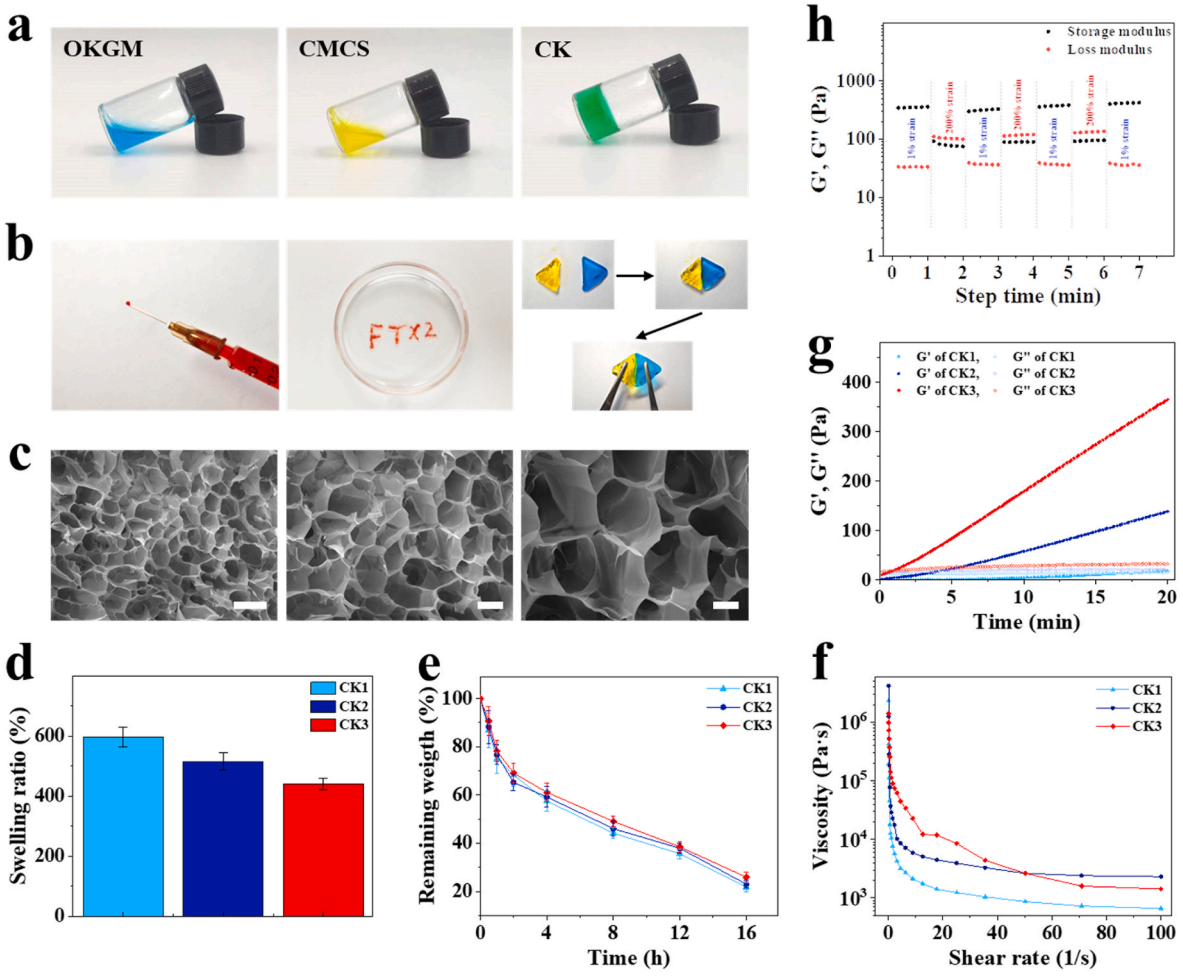

Fig. 2. Preparation and characterization of CK hydrogel. (a) CK hydrogels were formed by mixing OKGM and CMCS. (b) Demonstration of macroscopic injectability and self-healing properties of CK hydrogel. (c) SEM images of CK hydrogel; the scale bars are 100, 50, and 25 μm. (d) Swelling properties of CK hydrogels at different concentrations. (e) Degradation properties of CK hydrogels at different concentrations. (f) Shear-thinning properties of CK hydrogels. (g) Rheological properties of CK hydrogels. (h) Step strain testing of CK hydrogels at alternating strains of 1 % and 200 %.

absorb trauma exudates, and provide a suitable moist microenvironment for trauma healing. KGM, as an extremely hydrophilic natural polysaccharide, ensures that the hydrogels it forms have good water absorption properties. The hydrophilic and swelling properties of the hydrogels were evaluated by analyzing the swelling rate of the CK hydrogels in phosphate-buffered saline (PBS). Hydrogels with different concentrations showed good swelling performance in PBS (Fig. 2d). Specifically, the swelling rate of the hydrogels gradually decreased as the concentration of the formulated hydrogels increased, which may be related to a decrease in the number of hydrogel pores after intensive crosslinking of the hydrogels at high concentrations. Degradability is an important parameter in skin wounds. Owing to the short healing cycle of skin wounds, hydrogels must degrade rapidly in a short period to enable the release of the loaded drug (Fig. 2e). Different concentrations of CK hydrogels were able to degrade faster. At 16 h, the remaining weight of the hydrogel was approximately 20 %.

2.1.6. Rheological performance of hydrogels

The rheological properties of hydrogels include parameters such as mechanical strength, viscosity, and microscopic gelation time, which are crucial for their application on traumatic surfaces. The results of the rheometer tests in oscillation mode showed that the viscosity of each hydrogel group decreased with increasing rotational speed (Fig. 2f), indicating that the CK hydrogels had good injectability. Additionally, the frequency scan experiment showed that all groups of CK hydrogels gelled within 20 min. The hydrogel of the CK-1 group exhibited a gel state with a storage modulus (G′) > loss modulus (G″) at 67 s. Lastly, the mechanical properties of the hydrogels increased with increasing crosslinking time, and G′ was close to 400 pa after 20 min of reaction (Fig. 2g).

The introduction of the drug may affect the rheological properties of the hydrogels [36]. Therefore, we further examined the rheological properties of CK hydrogels loaded with BBR and Exo. Notably, the self-repairing hydrogels after drug loading showed slight changes in all aspects of rheological properties; they exhibited a faster gelation rate and appeared in a gel state at 40 s (Fig. S3). In addition, there was no change in terms of self-healing properties and shear-thinning properties of the drug-loaded hydrogels (Fig. S4 and Fig. S5). The hydrogel showed a change in rheological properties; this was mainly due to the introduction of the weakly alkaline BBR, which upregulated the pH value of the crosslinking microenvironment of the self-repairing hydrogel. The Schiff base bonds in the weakly alkaline environment crosslinked better, facilitating faster gel formation. However, this microenvironment change did not affect the other rheological properties of the hydrogel.

2.1.7. Self-healing performance of hydrogels

Owing to the prolonged exposure of hydrogel materials applied to skin wounds to external factors, the hydrogel will inevitably be damaged by the patient's movement and external forces. A self-healing hydrogel with Schiff base bonding can be spontaneously repaired by reversible covalent bonding, which prolongs the service life of the hydrogel and promotes better wound healing. The alternating stress scan experiment using the rheometer showed that with the sudden increase in stress, the G′ value was instantaneously lower than G″, indicating that the hydrogel was damaged and changed from a solid to a liquid state. However, with the release of 200 % stress, the G′ value of the hydrogel was higher than the G″ value, indicating that the hydrogel regained its gel state (Fig. 2h). Through successive alternating stress experiments, we showed that the hydrogel could connect to accept stress change rapidly and recover the original gel form after the stress disappeared. These experiments showed that the CK hydrogels exhibited efficient self-healing properties.

2.1.8. Loading of exos in hydrogels

The uniform distribution of Exos in hydrogels is the basis for the stable biological function of Exos. The cross-linking of KGM and CMCS to form a hydrogel is biocompatible with a loose pore structure that facilitates the loading and attachment of Exos. The distribution of Exos in the self-repairing hydrogel after immunofluorescence labeling was directly observed using fluorescence microscopy (Fig. S6). The Exos were uniformly distributed in the fluorescently colored hydrogel with no agglomeration or other phenomena. Therefore, Exos could be labeled by specific immunofluorescence and distributed uniformly in the CK@BBR&Exo hydrogel.

2.1.9. In vitro drug release of hydrogels

The sustained release of drugs in hydrogels facilitates their practical application in wound repair. Drug release from BBR in hydrogels was determined using UV spectrophotometry. *In vitro* experiments showed that BBR loaded into the hydrogels was continuously released in PBS at 37 °C. In the early stage, the BBR release rate was higher, which may be related to the faster degradation rate of the hydrogel in PBS. The drug release of BBR gradually stabilized with time. At 72 h, the cumulative drug release rate of BBR from the hydrogel was approximately 70 % (Fig. S7).

2.2. Characterization of exos

The particle size of the extracted Exos was analyzed using direct nanoparticle tracking analysis (NTA). The extracted ADSC-Exos were homogeneous in solution, with particle sizes mainly ranging from 100 to 250 nm (Fig. S8a). Furthermore, we observed Exos directly after negative staining using transmission electron microscopy (TEM); the Exo components were consistent with the NTA results (Fig. S8b). Additionally, the western blotting results showed high expression levels of TSG101 and CD81 associated with Exos (Fig. S8c). These experimental results indicated that Exos were successfully extracted from adipose stem cells.

2.3. Antimicrobial performance of CK@BBR

With the development of skin wound infections, bacterial activity can exacerbate inflammatory responses and delay wound repair. Moreover, if bacteria enter the bloodstream through a wound, they can cause a systemic bacterial infection response, endangering the patient's life. Therefore, hydrogels with antibacterial properties are necessary for the treatment of infected skin wounds. The hydrogel groups CK, CK@BBR1, CK@BBR2, and CK@BBR3 exhibited good antibacterial effects, mainly related to the CMCS and BBR components of the hydrogel system (Fig. 3a). CK@BBR showed a stronger antimicrobial effect with increasing BBR concentrations. Specifically, for *Escherichia coli*, the antimicrobial effect of each group of CK@BBR1, CK@BBR2, and CK@BBR3 was >90 %, with no significant difference. For *Staphylococcus aureus*, the antimicrobial effects of CK@BBR2 and CK@BBR3 groups exceeded 95 % and were not significantly different. Therefore, the drug concentration of the CK@BBR2 group was more suitable for application on infected skin wounds (Fig. 3b). Furthermore, SEM observations showed that *S. aureus* and *E. coli* treated with the blank control had good morphology; however, CK@BBR2 hydrogel-treated *S. aureus* and *E. coli* showed morphological and structural abnormalities compared with the blank control group (Fig. 3c). This indicated that the CK@BBR2 hydrogel had a good inhibitory and killing effect on *S. aureus* and *E. coli*.

2.4. Biocompatibility of CK@BBR&Exo

Biocompatibility is the most important indicator directly affecting the biological applications of hydrogel materials. Hydrogels based on cross-linking of two natural biomaterials, OKGM and CMCS, are the theoretical basis for ensuring good biocompatibility of hydrogel systems. We assessed the cytotoxicity of the hydrogels by determining the survival of human umbilical vein endothelial cells (HUVECs) after co-incubation with each hydrogel group using the Cell Counting Kit-8 (CCK-8) method; all cell groups survived (Fig. S9). Additionally, the

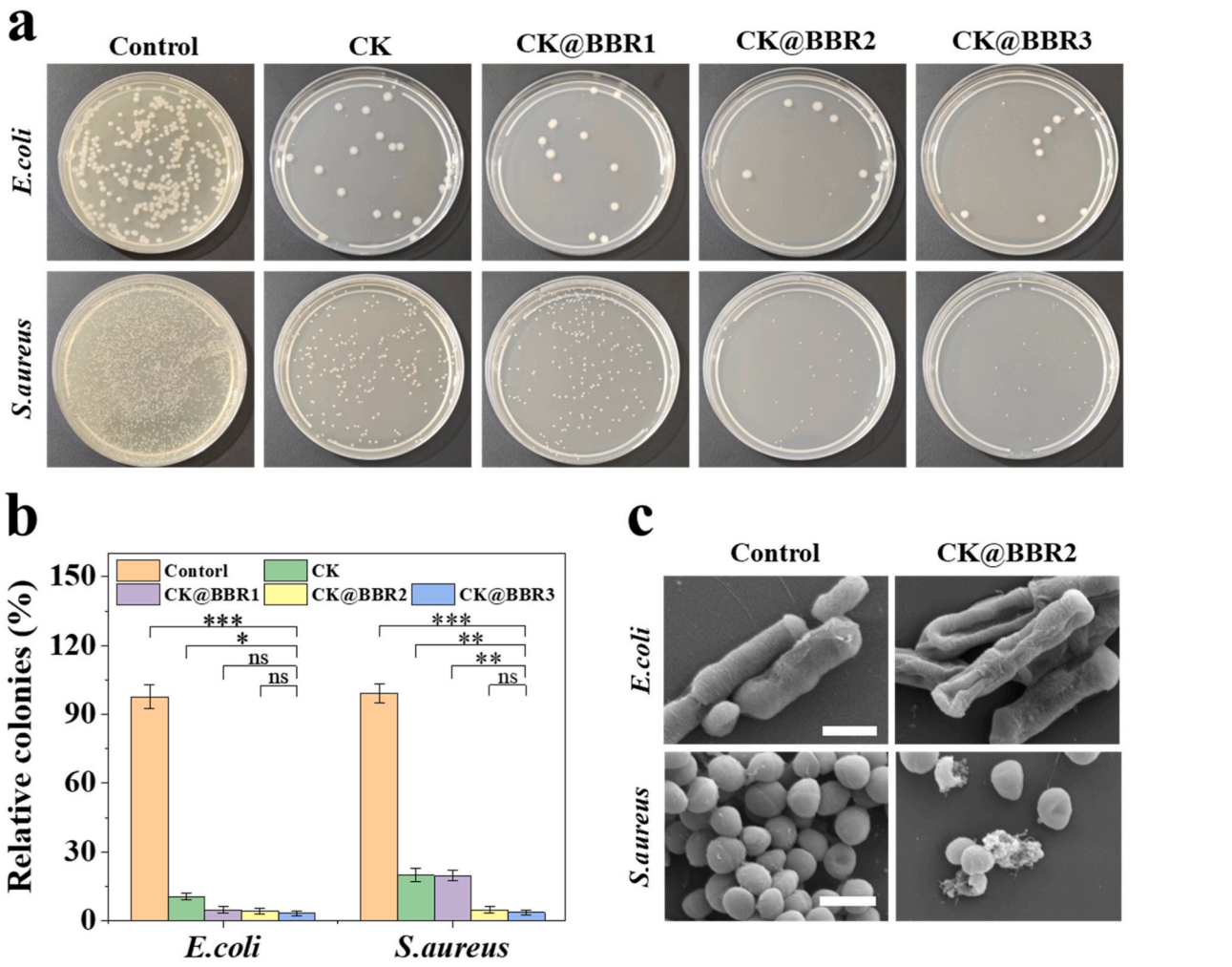

Fig. 3. Antimicrobial properties of CK@BBR hydrogels. (a) The antimicrobial properties of the groups were tested using the bacterial smear method. (b) Quantification of the bacterial smear plate count results for each group. (c) SEM images of the bacteria in the CK@BBR2 group; the scale bar is 1 μm. Groups with different letters indicate significant differences.

hemolysis test showed that all the hydrogel groups had good hemocompatibility (Fig. S10). These results indicated that the CK@BBR&Exo hydrogels had good biocompatibility.

2.5. *In vitro pro-angiogenic and pro-healing activities of CK@BBR&Exo*

Accelerated epithelialization of the wound surface promotes wound healing. In addition, accelerated vascularization of the wound surface facilitates the delivery of nutrients and oxygen to the wound surface, further promoting wound healing. In this study, the pro-angiogenic and pro-wound healing activities of Exos in hydrogels were investigated using scratch and tube formation assays. The scratch assay showed that the Exos-containing hydrogel significantly enhanced the migration of HUVECs (Fig. 4a and c), and Exos effectively induced cell migration. The blood vessel formation assay showed that the hydrogels containing Exos promoted the formation of blood vessels compared with the blank control group, and the effect of the hydrogel containing Exo was more obvious (Fig. 4b and d). This suggests that both Exos and BBR can promote neovascularization.

2.6. *In vivo wound healing and histological analysis of CK@BBR&Exo*

Wound healing involves several biological processes such as vascular regeneration, inflammatory responses, and collagen formation. To explore the healing effect of the CK@BBR&Exo hydrogel on infected skin wounds, we randomly grouped different infected wound rat models, treated the wounds with different hydrogel groups and PBS, and recorded the wound healing process of each group (Fig. 5a and c). The CK@BBR&Exo hydrogel group showed better wound healing and more mature epithelium and blood vessel formation, as observed using hematoxylin and eosin (H&E) staining, than the other groups (Fig. 5b and d). Moreover, all the experimental groups showed better healing effects than the blank control group, with respect to the drug components in each experimental group. Additionally, the healing effect of the CK@BBR group was better than that of CK@Exo, possibly related to the lack of biological activity of Exo owing to its degradation by bacteria on the wound surface.

2.7. *In vivo analysis of traumatic collagen deposition and inflammatory response induced by CK@BBR&Exo*

The deposition of collagen on the wound surface directly affects complete healing of the wound and scar formation. In this study, trabecular collagen deposition was detected using Masson staining. The highest collagen content was found in the CK@BBR&Exo group, and the collagen deposition content in the experimental groups was higher than that in the control group (Fig. 6a and b). Moreover, pro-inflammatory cytokine markers, interleukin-6 (IL-6), and tumor necrosis factor-α (TNF-α), were selected to investigate the inflammatory response of the trauma surface in different treatment groups. Immunohistochemical

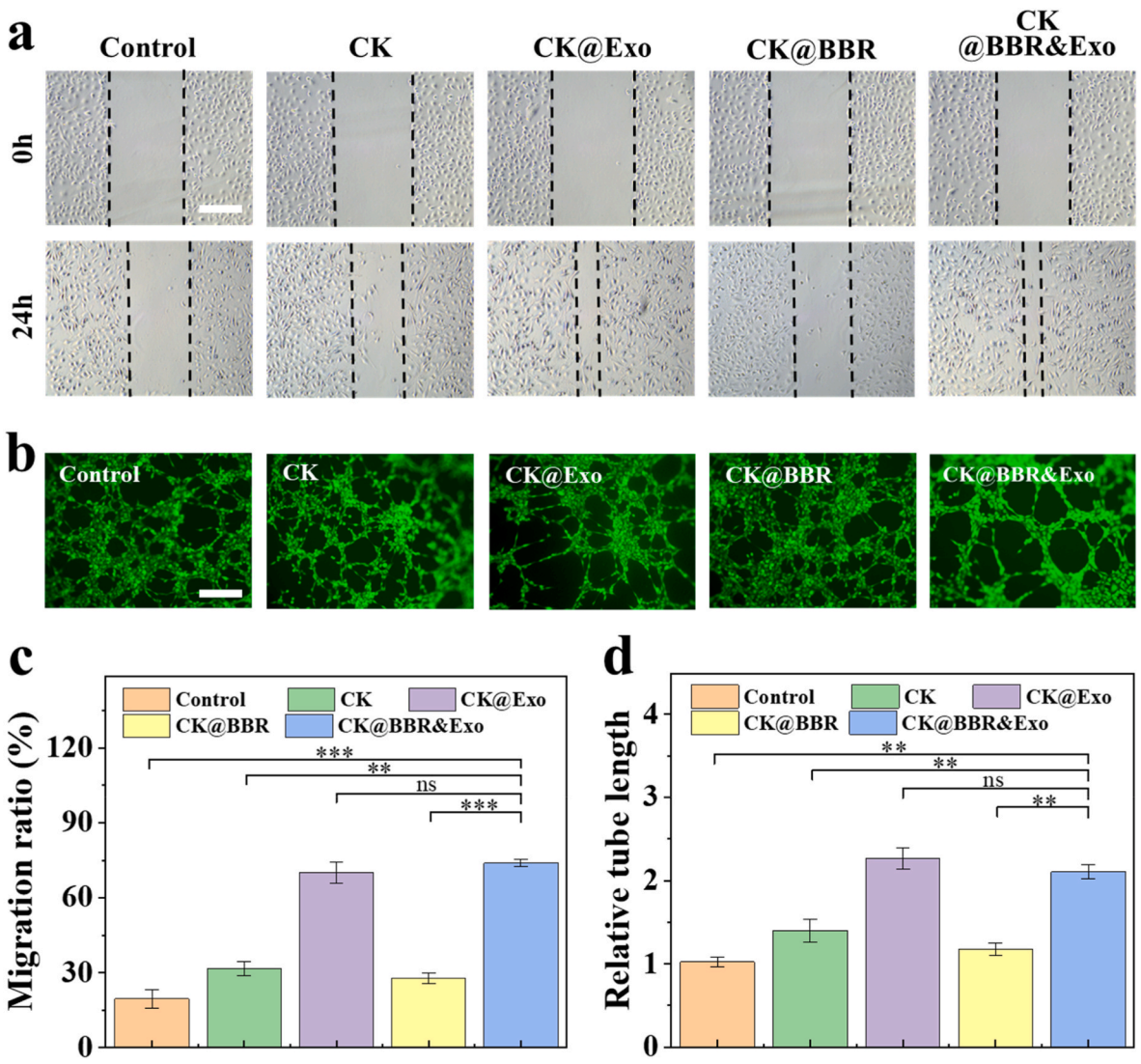

Fig. 4. Scratch and tube formation experiments. (a) HUVEC migration in different treatments. (b) HUVEC tube formation in different treatments. (c) Quantitative analysis of HUVEC migration. (d) Quantitative analysis of HUVEC tube formation. The scale bar is 200 μm. Groups with different letters indicate significant differences.

staining showed that the CK@BBR&Exo hydrogel effectively modulated the traumatic inflammatory activity and inhibited the expression of IL-6 and TNF-α (Fig. 6a, c, and 6d). This indicated that the CK@BBR&Exo hydrogel could effectively promote collagen deposition in infected wounds and promote wound healing by regulating the inflammatory activity of the wound.

2.8. *In vivo analysis of pro-angiogenesis induced by CK@BBR&Exo*

To further investigate the *in vivo* pro-angiogenic activity of the composite hydrogel against trauma, fluorescent staining was performed using CD31 and α-SMA to assess the level of trauma angiogenesis in different experimental groups. Fluorescence staining experiments showed that the CK@BBR&Exo group had a larger area of trauma immunofluorescence staining and greater vascular regeneration than the other groups (Fig. 7a). In addition, the expression of neovascularization-associated antibodies was higher in the CK@BBR&Exo group (Fig. 7b and c), confirming that the Exo component in the CK@BBR&Exo composite hydrogel mainly promoted trauma regeneration, consistent with the *in vitro* experiment results.

3. Conclusion

Wound infection is one of the most common complications associated with clinical trauma treatments. Infection can also greatly hinder the normal healing of wounds, causing symptoms such as fever, pain, sepsis, and even death. Therefore, correcting wound infection has always been the key to trauma treatment. CK@BBR&Exo multifunctional self-healing hydrogels for infected wounds were prepared based on Schiff base reversible covalent bonds using various natural materials. The CK@BBR&Exo composite hydrogel promoted rapid healing of infected skin wounds, leveraging its antibacterial, anti-inflammatory, and pro-angiogenic activities. Moreover, the hydrogel prepared based on the crosslinking of OKGM and CMCS exhibited good rheological, swelling, injectable, and self-healing properties. In this, OKGM as a polymer oxidized polysaccharide is indispensable for maintaining a more stable cross-linking network of hydrogels, providing good hydrophilicity and rheological properties, as well as biocompatibility, which are all favorable for the application of hydrogels in skin wounds. Meanwhile, CMCS also plays a good antimicrobial role to a certain extent. Compared with traditional dressings, this self-healing hydrogel can rapidly and completely adhere to and cover the wound via injection and absorb the wound exudate to provide a suitable microenvironment

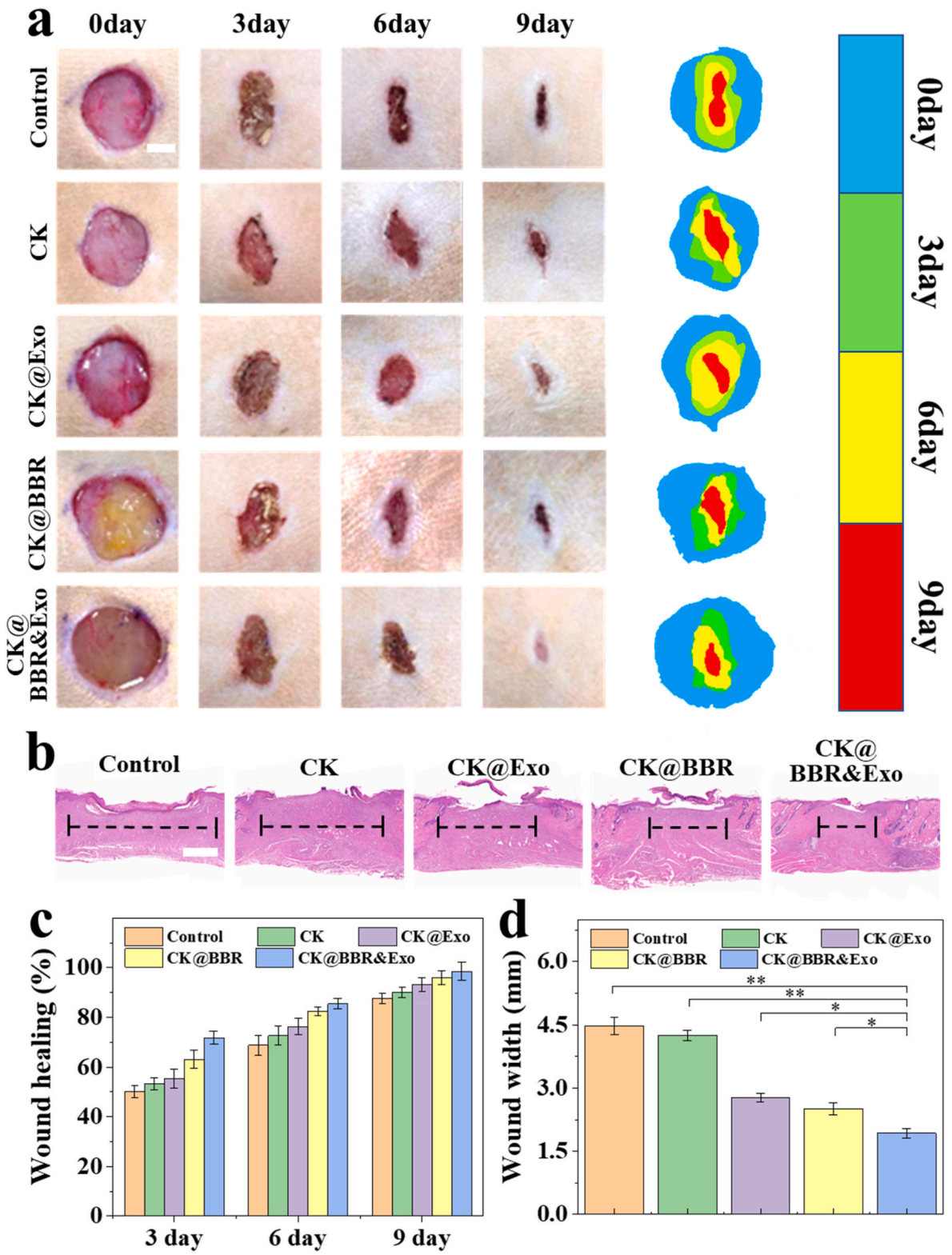

Fig. 5. Wound healing and histological analysis. (a) Representative wounds in different groups; the scale bar is 500 mm. (b) H&E staining of different groups; the scale bar is 1 mm. (c) Quantitative analysis of wound healing. (d) Quantitative analysis of tissue width. Groups with different letters indicate statistically significant differences.

for the wound. The results demonstrated that the CK@BBR&Exo self-healing hydrogel could promote the healing of infected wounds in rats by rapidly inhibiting and killing trauma bacteria, regulating the inflammatory response, and promoting vascular regeneration and epithelialization. This indicates the research and commercial values of this self-repairing hydrogel.

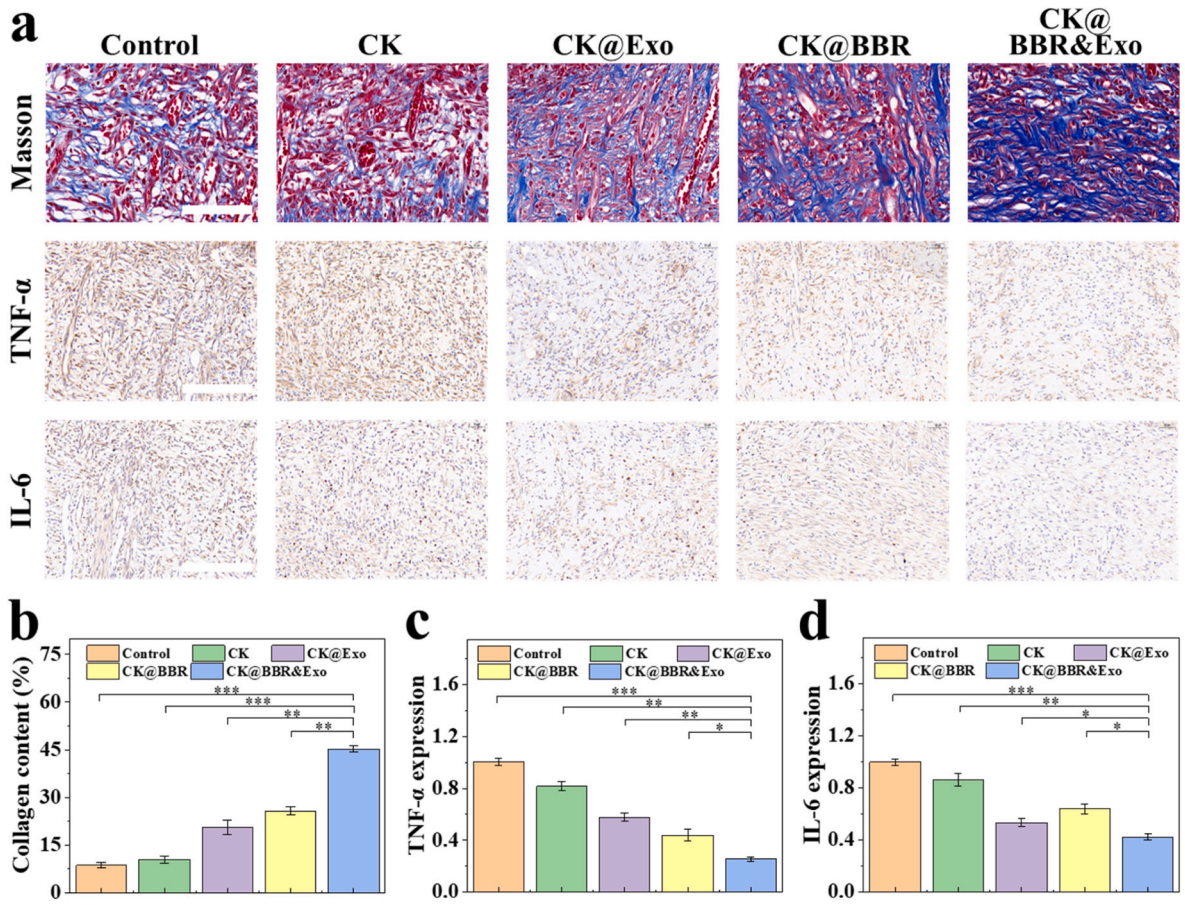

Fig. 6. Analysis of collagen deposition and pro-inflammatory factors in wounds. (a) Staining of collagen, TNF-α, and IL-6. (b–d) Quantitative analysis of collagen deposition, TNF-α, and IL-6 in different groups. The scale bars are 100, 200, and 200 μm. Groups with different letters indicate significant differences.

4. Methods and materials

4.1. Materials

KGM, CMCS (≥90 % deacetylated), sodium periodate, ethylene glycol, ethanol, tert-butanol, and other chemicals, such as glutaraldehyde, were purchased from Maclean's Biotech (Shanghai, China); all chemicals were not further purified. Masson's trichrome and H&E staining kits were purchased from Servicebio (Wuhan, China). All aqueous solutions were prepared using distilled water (dH_2O) via double evaporation. Additionally, human umbilical vein endothelial (HUVEC) cells were purchased from Servicebio, and cells were passaged for over three generations. Calcein-AM/PI and CCK-8 were purchased from Keygen Biotech Company (Nanjing, China). Moreover, DMEM plates, DMEM/F12 plates, and PBS for cell culture were obtained from HyClone (Logan, Utah, USA), and Matrigel was purchased from BD Bioscience (Shanghai, China). The antibodies used in the experiments were purchased from Abcam (Cambridge, UK), and male Sprague–Dawley (SD) rats (200–220 g) were purchased from Slaughter Kingda Laboratory Animal Co. (Hunan, China). Furthermore, the rats were housed in a suitable environment with free access to food and water. The Animal Experimentation Ethics Committee of the Xiangya Second Hospital of Central South University approved all animal care and experimental procedures (Approval No. 20230618).

4.2. Preparation of OKGM

We used a previously described method with some modifications [25]. First, 5 g of KGM was dissolved in 500 mL dH_2O and heated in a water bath at 40 °C with stirring. After KGM was completely dissolved, 10 mL of sodium periodate (0.35 g/mL) was added dropwise and stirred for 6 h at 37 °C under dark conditions. Next, ethylene glycol (25 mL) was added to terminate the reaction, and the mixture was stirred for 2 h. Subsequently, the mixture was dialyzed using a dialysis membrane (MWCO: 10 K–12 K) in dH_2O for 3 days, during which the dH_2O was changed every 6 h until the dialysate was iodate-free. Lastly, the dialyzed liquid was centrifuged at 1000×*g* for 15 min, and the supernatant was freeze-dried to obtain purified OKGM.

4.3. Extraction and characterization of ADSC-Exos

The Exos were extracted through ultracentrifugation. After the third to fifth generation, ADSCs were cultured without serum for 72 h. The supernatant was collected and centrifuged at 2000×*g* and 4 °C for 30 min. The supernatant was collected, centrifuged at 20,000×*g* and 4 °C for 60 min, and re-centrifuged at 100,000×*g* for 60 min. Subsequently, the precipitate at the bottom of the super-dissociation tube was collected, diluted with PBS, and centrifuged at 100,000×*g* for 60 min. Finally, the collected precipitate was resuspended in 100 μL PBS, dispensed, and stored at −80 °C for subsequent experiments. The morphology and particle size of Exos were characterized using TEM and NTA, respectively. Additionally, the expression levels of TSG101 and CD81 in the extracted Exos were determined using western blotting.

4.4. Preparation of CK@BBR&Exo hydrogels

A quantity of CMCS powder was added to the PBS solution and heated in a water bath at 40 °C with constant stirring until a final CMCS concentration of 3 wt% was obtained. In addition, an appropriate amount of OKGM powder was dissolved in PBS by heating in a water

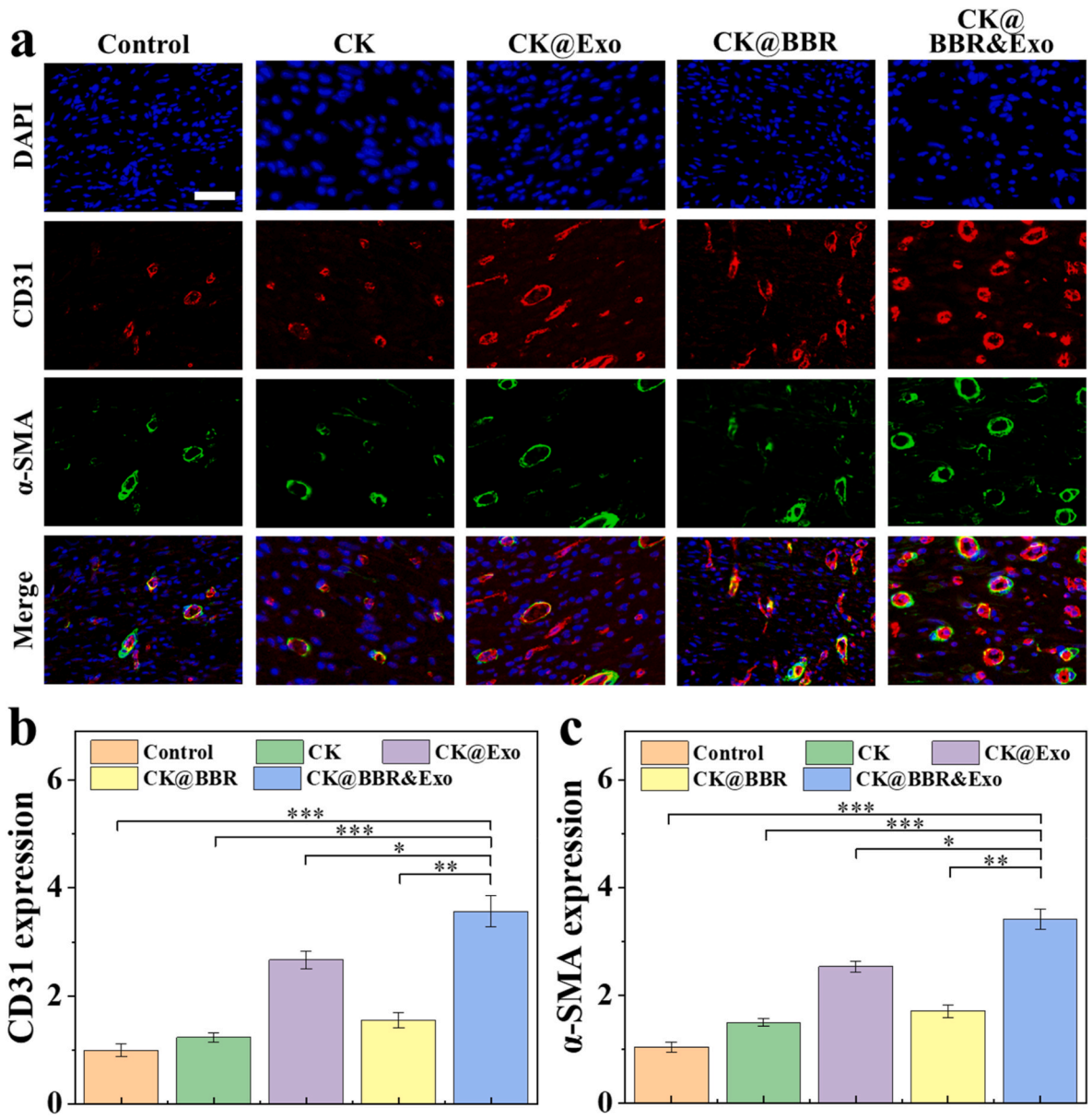

Fig. 7. Wound neovascularization analysis. (a) Fluorescent staining of neovascularization; the scale bar is 50 μm. (b, c) Quantitative analysis of α-SMA and CD31 in different groups. Groups with different letters indicate statistically significant differences.

bath at 40 °C to obtain final OKGM solutions of 1.5, 3, and 6 wt%. Subsequently, 1 mL of CMCS solution was homogeneously mixed with an equal volume of each OKGM solution to obtain different concentrations of CK hydrogels. The hydrogels formed lasted for a period of time at 25 °C and were characterized. The CK hydrogel samples included CK1 = 1.5 % OKGM: 3 % CMCS, CK2 = 3 % OKGM: 3 % CMS, and CK3 = 6 % OKGM:3 % CMCS.

Similarly, we prepared a CMCS solution by adding different amounts of BBR powder to ensure that the concentration of BBR in the precursor solution was 0.5, 1.0, and 1.5 mg/mL. Subsequently, we added equal volumes of OKGM solution and mixed them homogeneously, to obtain three sets of hydrogels with different drug concentrations for CK@BBR1, CK@BBR2, and CK@BBR3, respectively. Finally, we added 100 μL Exo to the existing hydrogel system of BBR composition to introduce Exos into the hydrogel system. The composite hydrogels CK@BBR&Exo were successfully prepared.

4.5. Characterization of hydrogels

4.5.1. FTIR measurements

IR spectra of KGM and OKGM were measured and analyzed using an IR spectrophotometer (Nicolet-6700, Thermoelectric, China). Briefly, the powder of each polymer was ground into fine and uniform particles without large or hard particles, and the mass of each group was not <20 mg. Finally, the IR spectra of each powder sample were detected using the IR spectrophotometer in the wave number range of 4000–500 cm^{-1} at 25 °C. The resolution was set at 4 cm^{-1}, and the spectra were recorded in 32 scans.

4.5.2. NMR measurements

D_2O was used as a solvent to fully dissolve OKGM. Then, ^1H NMR of OKGM was detected using NMR equipment (Bruker Ascend 400 MHz). Finally, the NMR data of OKGM were obtained and processed to draw the images.

4.5.3. Topography analysis

The microscopic morphology of the CK3 hydrogels was observed using SEM. Specifically, the prepared columnar CK3 hydrogels were freeze-dried to obtain lyophilized hydrogel samples. The freeze-dried samples were cut vertically into cylindrical shapes (10 mm in diameter and 5 mm in height) using a thin blade, and a layer of gold was sprayed on the cut cross-section of the samples. After vacuum spraying, the morphology of the composite hydrogel was observed directly using SEM at 20 kV. The magnification of the SEM images was continuously adjusted to observe the fine structure of the hydrogels.

4.5.4. Swelling and degradation measurements

Crosslinked cylindrical hydrogel samples (15 mm in diameter and 10 mm in height) of different concentrations were freeze-dried, and their weights were measured. The samples were immersed in PBS and stored at 37 °C. The hydrogel samples were removed from the PBS, excess liquid was aspirated from the surface samples with filter paper, and the hydrogel was weighed at 1-h intervals for 48 consecutive hours. After weighing, the hydrogels were placed back into PBS buffer, with continuous weight monitoring. The maximum weight of the hydrogel was recorded. The swelling ratio (SR) was calculated as follows:

$$SR = (W_s\text{-}W_d) / W_d \times 100\%$$

where W_s and W_d are the weights of the samples in swollen and dry states, respectively.

Finally, the fully crosslinked hydrogel was placed in PBS solution at 37 °C. The weight of the hydrogel was measured continuously as described above until the hydrogel was completely degraded. The degradation rate was calculated as follows:

Remaining weight (%) = $(W_t\text{-}W_i)/W_i \times 100$ %, where W_i and W_t represent the initial weight of the wet gel and the wet weight at a predetermined time point, respectively.

4.5.5. Glue formation and macroscopic injectability determination

The gelation of hydrogels crosslinked into gels was determined using the vial tilt method [37]. Specifically, the hydrogels were prepared using the method described above, and the reactants were uniformly mixed in uniform-sized vials to fully crosslink the hydrogels. The hydrogel after gelation was extracted using a 1 mL medical syringe, and the stained hydrogel was injected into the culture plate using a medical needle, through which special patterns were drawn to verify its injectability.

4.5.6. Measurement of rheological performance

The rheological properties of different experimental groups of hydrogels were determined using two modes. Briefly, the reactants required to prepare self-healing hydrogels were mixed and crosslink ed directly on a rheometer sample stage with a final volume of 1 mL. The samples were measured using a rheometer (Smartpave, Anton Paar) in oscillation mode at 37 °C (parameter settings: gap size = 1 mm, strain = 1.0 %, and frequency = 10 Hz). Additionally, G′ and G″ of the hydrogels of different experimental groups were measured continuously, and the time point at which G′ was >G″ was the time at which the hydrogels gelled.

4.5.7. Self-repair performance measurement

The self-healing properties of the hydrogels were evaluated via macroscopic observation and rheometry, using the CK3 group as an example. First, hydrogels were prepared in rubber molds using the proportions of the CK3 experimental group. Next, 10 μL of yellow pigment (food grade) was added to the hydrogels to facilitate observation, and the hydrogels were cut in the middle. The approach used for the other half of the blue-stained hydrogels was applied, and the two cut hydrogels were allowed to reconstitute at 25 °C for 4 h without external intervention. Next, the self-healing properties of the hydrogels were analyzed macroscopically by direct observation of the stretching of the reconstituted hydrogels.

The rheological performance of the hydrogels under alternating stress was used to further evaluate their self-healing properties. The alternating strain was set to change from γ = 1 % to a high strain (γ = 200 %) for 360 s at each strain interval, and a fixed continuous step strain angular frequency (10 rad/s) was measured. The amplitude oscillatory strains were then switched from low to high at each 60 s strain interval.

4.5.8. Detection of exo loading in hydrogels

Exos were labeled according to the manufacturer's instructions of the PKH67 kit (Sigma). The labeled Exo and CK@BBR hydrogels were mixed thoroughly and evenly in an ice bath to obtain CK@BBR&Exo hydrogel. The resulting composite hydrogel was stored at 4 °C. A 12-well plate was directly and evenly covered with a layer of hydrogel. The dispersion of Exos in the hydrogel was directly observed using a fluorescence microscope.

4.5.9. Measurement of BBR release in vitro

The *in vitro* drug release of BBR from hydrogels was determined using UV absorption spectroscopy. The hydrogel was placed in a dialysis bag and 100 mL PBS was added; the sample was incubated at 37 °C. Drug release from the hydrogel was determined continuously at 340 nm using a UV spectrophotometer (Multiskan SkyHigh, China).

4.6. In vitro antimicrobial measurement

Two representative strains of *E. coli* and *S. aureus* were used for antibacterial experiments. First, appropriate amounts of *E. coli* or *S. aureus* strains were transferred to Luria–Bertani (LB) liquid medium and incubated for 6 h. The bacterial suspension was serially diluted with LB liquid medium to a concentration of 1×10^6 CFU/mL. Subsequently, 200 μL each of CK, CK@BBR1, CK@BBR2, and CK@BBR3 hydrogels and PBS were mixed with the diluted bacterial suspension and incubated in a bacterial incubator for 6–8 h. Subsequently, the bacterial suspensions were evenly spread on solid (LB) agar plates (Servicebio) using a bacterial applicator stick, and the LB agar plates were incubated at 37 °C for 12 h. Finally, the bacteria in the LB agar plates were counted and analyzed for each group. The experiment was repeated more than three times.

Bacterial suspensions from the blank group were injected into six-well plates after co-incubation with the CK@BBR2 hydrogels. Cell crawlers were placed in six-well plates and co-incubated with the bacterial suspension in a bacterial incubator for >12 h to ensure that they were inoculated with bacteria from the different experimental groups. The bacteria crawls were fixed with 2.5 % glutaraldehyde for 8 h and rinsed thrice with PBS. Subsequently, gradient dehydration was performed once using 30, 50, 70, 80, and 90 % ethanol and twice using anhydrous ethanol for 15–20 min each. The crawl sheets were soaked in tert-butanol for 20 min. Finally, the crawl sheets were gold-sprayed and vacuum sprayed, and the morphology of each group of bacteria was observed using SEM at 10 kV.

4.7. In vitro cytotoxicity measurement

The cytotoxicity of the CK@BBR&Exo hydrogels in HUVECs was investigated using CCK-8. First, the reactant powder for synthesizing the hydrogels was sterilized using sufficient UV light irradiation, and CK hydrogels, hydrogels loaded with BBR (CK@BBR), hydrogels loaded with Exo (CK@Exo), and CK@BBR&Exo hydrogels were synthesized under aseptic conditions. Next, HUVECs at a density of 0.5×10^4 mL^{-1} were inoculated on 96-well plates with 10 μL each of PBS and CK, CK@BBR, CK@Exo, and CK@BBR&Exo hydrogels and co-incubated at 37 °C, and 5 % CO_2. After 3 days of incubation, the Calcein-AM/PI staining kit was added and incubated for 10 min in the dark. Images were obtained using a fluorescence microscope (Olympus). CCK-8

solution (10 μL) was added, and the optical density was measured at 450 nm. The experiment was repeated more than three times.

4. 8. In vitro angiogenesis measurement

HUVECs were used for the *in vitro* tube formation experiments. First, 96-well plates were evenly coated with Matrigel, and HUVECs of the fourth to seventh generation (cell density 1×10^4) were selected, inoculated in the well plates, and incubated with each group of hydrogel leaching solution in 50 μL of serum-free alkaline medium for 8 h. Calcein-AM staining was then performed for 20 min, and the stain was removed using PBS. Finally, fluorescence images were captured using an inverted fluorescence microscope. The ImageJ software was used to analyze angiogenesis, and the relative tube length was calculated using the control group. The experiments were repeated more than three times.

4. 9. In vitro hemolysis measurement

Rat whole blood was collected in anticoagulation tubes. Whole blood was washed repeatedly with PBS to obtain a clean erythrocyte suspension. Using PBS for dilution, dH_2O, PBS, and each group of hydrogels were incubated with the diluted erythrocyte solution for 6 h at 37 °C. Finally, the samples were centrifuged at 500×*g* for 3 min and hemolysis was determined for each group. The experiment was repeated more than three times.

4.10. Cell migration measurement

The leaching solution from the hydrogels of each group was evenly distributed in Petri dishes and co-cultured with HUVECs. After the cell layer was successfully formed in the culture plate, the fused cell layer was slowly scratched in a straight line using a sterilized gun tip. The width of the scratch was then observed using light microscopy and recorded for each group. The culture was continued for 12 h to observe the migration of HUVECs on the culture plate. The cell migration rate was calculated by comparing scratch widths before and after cell migration in each experimental group. The experiment was repeated more than three times.

4.11. In vivo wound healing measurement

Adult SD rats ($n = 3$) were selected to construct a full skin infection wound model to evaluate the wound healing ability of the CK@BBR&Exo hydrogel. First, the rats were anesthetized with isoflurane via inhalation using an anesthesia ventilator. Next, a full-thickness trauma layer with a diameter of 1 cm was created on the back of the rats, and 200 μL of *S. aureus* bacterial suspension was injected at the trauma site to form an infected trauma. Subsequently, the rat skin trauma was treated with CK, CK@BBR, CK@Exo, and CK@BBR&Exo hydrogels and PBS. Dorsal trauma of the rats was recorded on days 0, 3, 6, and 9 using a digital camera, and the data were analyzed. The rats were sacrificed on day 9, and traumatic granulation tissue was collected from each group for subsequent experimental analysis.

4.12. Histological, immunohistochemical, and fluorescent staining measurements

The collected traumatized skin samples were embedded in paraffin and dehydrated using an ethanol gradient. Subsequently, the samples were cut into 5 μm thick serial sections using a microtome. Next, the sections were stained with H&E and Masson's trichrome, and epithelialization and collagen deposition during wound healing were assessed by observing the staining results. Additionally, the inflammatory response of the wounds was assessed by immunohistochemical staining using IL-6 and TNF-α. Finally, CD31 and α-SMA fluorescence staining were used to assess trauma neovascularization.

4.13. Data analysis

The experimental data are expressed as mean ± standard deviation ($n \geq 3$). Significant differences between the two groups were tested using the Student's t-test; multiple comparisons were assessed using analysis of variance models. Significant differences were considered if $^*p < 0.05$, $^{**}p < 0.01$, and $^{***}p < 0.001$.

Credit statement

Pu Yang and Yikun Ju: Investigation, Writing- Original draft preparation. **Xiangjun Liu and Zhen Li:** Writing - Review & Editing. **Hairong Liu, Mengni Yang and Xin Chen:** Formal analysis and Data Curation. **Lanjie Lei and Bairong Fang:** Conceptualization and Methodology.

Declaration of competing interest

The authors declare no conflict of interest.

Data availability

Data will be made available on request.

Acknowledgements

This study was funded by the Natural Science Foundation of Hunan Province, China (No. 2021JJ30928) and Scientific Research Project of Hunan Provincial Health Commission , China (No. C202304106744).

Appendix A. Supplementary data

Supplementary data to this article can be found online at https://doi.org/10.1016/j.mtbio.2023.100875.

References

[1] L. Gravitz, Skin, Nature 563 (7732) (2018) S83.
[2] G. Theocharidis, H. Yuk, H. Roh, L. Wang, I. Mezghani, J. Wu, A. Kafanas, M. Contreras, B. Sumpio, Z. Li, E. Wang, L. Chen, C.F. Guo, N. Jayaswal, X. L. Katopodi, N. Kalavros, C.S. Nabzdyk, I.S. Vlachos, A. Veves, X. Zhao, A strain-programmed patch for the healing of diabetic wounds, Nat. Biomed. Eng. 6 (10) (2022) 1118–1133.
[3] B.K. Sun, Z. Siprashvili, P.A. Khavari, Advances in skin grafting and treatment of cutaneous wounds, Science 346 (6212) (2014) 941–945.
[4] M. Rodrigues, N. Kosaric, C.A. Bonham, G.C. Gurtner, Wound healing: a cellular perspective, Physiol. Rev. 99 (1) (2019) 665–706.
[5] D.Y. Matar, B. Ng, O. Darwish, M. Wu, D.P. Orgill, A.C. Panayi, Skin inflammation with a focus on wound healing, Adv. Wound Care 12 (5) (2023) 269–287.
[6] H. Jo, S. Brito, B.M. Kwak, S. Park, M.G. Lee, B.H. Bin, Applications of mesenchymal stem cells in skin regeneration and rejuvenation, Int. J. Mol. Sci. 22 (5) (2021) 2410.
[7] B. Guo, R. Dong, Y. Liang, M. Li, Haemostatic materials for wound healing applications, Nat. Rev. Chem 5 (11) (2021) 773–791.
[8] F. Mas-Celis, J. Olea-López, J.A. Parroquin-Maldonado, Sepsis in trauma: a deadly complication, Arch. Med. Res. 52 (8) (2021) 808–816.
[9] G.R. Lee, D. Gallo, R.W. Alves de Souza, S. Tiwari-Heckler, E. Csizmadia, J. D. Harbison, S. Shankar, V. Banner-Goodspeed, M.B. Yaffe, M.S. Longhi, C. J. Hauser, L.E. Otterbein, Trauma-induced heme release increases susceptibility to bacterial infection, JCI Insight 6 (20) (2021), e150813.
[10] R. Cui, L. Zhang, R. Ou, Y. Xu, L. Xu, X.Y. Zhan, D. Li, Polysaccharide-based hydrogels for wound dressing: design considerations and clinical applications, Front. Bioeng. Biotechnol. 10 (2022), 845735.
[11] W. Liao, X. Duan, F. Xie, D. Zheng, P. Yang, X. Wang, Z. Hu, 3d-bioprinted double-crosslinked angiogenic alginate/chondroitin sulfate patch for diabetic wound healing, Int. J. Biol. Macromol. 236 (2023), 123952.
[12] Y. Yu, Y. Gao, L. He, B. Fang, W. Ge, P. Yang, Y. Ju, X. Xie, L. Lei, Biomaterial-based gene therapy, MedComm 4 (3) (2020) e259, 2023.
[13] L. Yang, X. Wang, Y. Yu, L. Shang, W. Xu, Y. Zhao, Bio-inspired dual-adhesive particles from microfluidic electrospray for bone regeneration, Nano Res. 16 (4) (2023) 5292–5299.

[14] L. Quan, Y. Xin, X. Wu, Q. Ao, Mechanism of self-healing hydrogels and application in tissue engineering, Polymers 14 (11) (2022) 2184.
[15] R. Haghniaz, H. Montazerian, A. Rabbani, A. Baidya, B. Usui, Y. Zhu, M. Tavafoghi, F. Wahid, H.J. Kim, A. Sheikhi, A. Khademhosseini, Injectable, antibacterial, and hemostatic tissue sealant hydrogels, Adv. Healthcare Mater. (2023), e2301551.
[16] Z. Obagi, G. Damiani, A. Grada, V. Falanga, Principles of wound dressings: a review, Surg. Technol. Int. 35 (2019) 50–57.
[17] Y. Liang, J. He, B. Guo, Functional hydrogels as wound dressing to enhance wound healing, ACS Nano 15 (8) (2021) 12687–12722.
[18] Y. Xu, Y. Li, Q. Chen, L. Fu, L. Tao, Y. Wei, Injectable and self-healing chitosan hydrogel based on imine bonds: design and therapeutic applications, Int. J. Mol. Sci. 19 (8) (2018) 2198.
[19] P. Bertsch, M. Diba, D.J. Mooney, S.C.G. Leeuwenburgh, Self-healing injectable hydrogels for tissue regeneration, Chem. Rev. 123 (2) (2023) 834–873.
[20] B.D. Zheng, J. Ye, Y.C. Yang, Y.Y. Huang, M.T. Xiao, Self-healing polysaccharide-based injectable hydrogels with antibacterial activity for wound healing, Carbohydr. Polym. 275 (2022), 118770.
[21] S. Rashki, K. Asgarpour, H. Tarrahimofrad, M. Hashemipour, M.S. Ebrahimi, H. Fathizadeh, A. Khorshidi, H. Khan, Z. Marzhoseyni, M. Salavati-Niasari, H. Mirzaei, Chitosan-based nanoparticles against bacterial infections, Carbohydr. Polym. 251 (2021), 117108.
[22] A. Muxika, A. Etxabide, J. Uranga, P. Guerrero, K. de la Caba, Chitosan as a bioactive polymer: processing, properties and applications, Int. J. Biol. Macromol. 105 (Pt 2) (2017) 1358–1368.
[23] S. Ye, A.W. Zongo, B.R. Shah, J. Li, B. Li, Konjac glucomannan (kgm), deacetylated kgm (da-kgm), and degraded kgm derivatives: a special focus on colloidal nutrition, J. Agric. Food Chem. 69 (44) (2021) 12921–12932.
[24] Y. Wang, R. Xie, Q. Li, F. Dai, G. Lan, S. Shang, F. Lu, A self-adapting hydrogel based on chitosan/oxidized konjac glucomannan/agnps for repairing irregular wounds, Biomater. Sci. 8 (7) (2020) 1910–1922.
[25] L. Fan, J. Yi, J. Tong, X. Zhou, H. Ge, S. Zou, H. Wen, M. Nie, Preparation and characterization of oxidized konjac glucomannan/carboxymethyl chitosan/graphene oxide hydrogel, Int. J. Biol. Macromol. 91 (2016) 358–367.
[26] P. Luo, M. Nie, H. Wen, W. Xu, L. Fan, Q. Cao, Preparation and characterization of carboxymethyl chitosan sulfate/oxidized konjac glucomannan hydrogels, Int. J. Biol. Macromol. 113 (2018) 1024–1031.
[27] K. Wang, X. Feng, L. Chai, S. Cao, F. Qiu, The metabolism of berberine and its contribution to the pharmacological effects, Drug Metab. Rev. 49 (2) (2017) 139–157.
[28] D. Song, J. Hao, D. Fan, Biological properties and clinical applications of berberine, Front. Med. 14 (5) (2020) 564–582.
[29] J. Tong, X. Hou, D. Cui, W. Chen, H. Yao, B. Xiong, L. Cai, H. Zhang, L. Jiang, A berberine hydrochloride-carboxymethyl chitosan hydrogel protects against staphylococcus aureus infection in a rat mastitis model, Carbohydr. Polym. 278 (2022), 118910.
[30] S. Rani, T. Ritter, The exosome - a naturally secreted nanoparticle and its application to wound healing, Adv. Mater. 28 (27) (2016) 5542–5552.
[31] Y. An, S. Lin, X. Tan, S. Zhu, F. Nie, Y. Zhen, L. Gu, C. Zhang, B. Wang, W. Wei, D. Li, J. Wu, Exosomes from adipose-derived stem cells and application to skin wound healing, Cell Prolif. 54 (3) (2021), e12993.
[32] M.T. Roefs, J.P.G. Sluijter, P. Vader, Extracellular vesicle-associated proteins in tissue repair, Trends Cell Biol. 30 (12) (2020) 990–1013.
[33] Y. Ju, Y. Hu, P. Yang, X. Xie, B. Fang, Extracellular vesicle-loaded hydrogels for tissue repair and regeneration, Mater Today Bio 18 (2023), 100522.
[34] J. Lin, Z. Wang, J. Huang, S. Tang, Q. Saiding, Q. Zhu, W. Cui, Microenvironment-protected exosome-hydrogel for facilitating endometrial regeneration, fertility restoration, and live birth of offspring, Small 17 (11) (2021), e2007235.
[35] C. Zhang, X. Yang, W. Hu, X. Han, L. Fan, S. Tao, Preparation and characterization of carboxymethyl chitosan/collagen peptide/oxidized konjac composite hydrogel, Int. J. Biol. Macromol. 149 (2020) 31–40.
[36] Q. Zong, X. Peng, Y. Ding, H. Wu, C. Lu, J. Ye, W. Sun, J. Zhang, Y. Zhai, Multifunctional hydrogel wound dressing with rapid on-demand degradation property based on aliphatic polycarbonate and chitosan, Int. J. Biol. Macromol. 244 (2023), 125138.
[37] Y. Jiang, J. Huang, X. Wu, Y. Ren, Z. Li, J. Ren, Controlled release of silver ions from agnps using a hydrogel based on konjac glucomannan and chitosan for infected wounds, Int. J. Biol. Macromol. 149 (2020) 148–157.